Geophysical Research Letters

RESEARCH LETTER
10.1029/2023GL106680

Critical Size of Silver Iodide Containing Glaciogenic Cloud Seeding Particles

Jie Chen[1], Carolin Rösch[1,2], Michael Rösch[1], Aleksei Shilin[3], and Zamin A. Kanji[1]

[1]Institute for Atmospheric and Climate Science, ETH Zürich, Zurich, Switzerland, [2]Now at City of Zurich, Environment and Health Safety, Air Quality Division, Zurich, Switzerland, [3]Cloud Seeding Technologies, Gaertringen, Germany

Key Points:

- Silver iodide (AgI) containing cloud-seeding aerosols exhibit comparable ice-forming abilities to pure AgI at sizes of 200 and 400 nm
- Non-AgI impurities produced from flare burning decrease the ice nucleation ability of particles smaller than 90 nm
- A new parameterization is presented to estimate the minimum mass of AgI particles required to maximize glaciogenic seeding

Supporting Information:

Supporting Information may be found in the online version of this article.

Correspondence to:

J. Chen and Z. A. Kanji,
jie.chen@env.ethz.ch;
zamin.kanji@env.ethz.ch

Citation:

Chen, J., Rösch, C., Rösch, M., Shilin, A., & Kanji, Z. A. (2024). Critical size of silver iodide containing glaciogenic cloud seeding particles. *Geophysical Research Letters*, *51*, e2023GL106680. https://doi.org/10.1029/2023GL106680

Received 4 OCT 2023
Accepted 18 MAR 2024

Author Contributions:

Conceptualization: Jie Chen, Zamin A. Kanji
Methodology: Jie Chen, Carolin Rösch, Michael Rösch, Aleksei Shilin, Zamin A. Kanji
Project administration: Jie Chen, Zamin A. Kanji
Supervision: Zamin A. Kanji
Writing – original draft: Jie Chen, Zamin A. Kanji
Writing – review & editing: Jie Chen, Zamin A. Kanji

Abstract Cloud seeding is considered a practical but unproved method to enhance precipitation or suppress hail, due to insufficient knowledge of ice formation and evolution after seeding clouds with ice nucleating particles. This study investigates the size effects on the immersion freezing of aerosol produced from commercial silver iodide (AgI) containing flares at mixed-phase cloud temperatures from 243 to 267 K. Flare-generated aerosol exhibited comparable ice nucleation ability (INA) to pure AgI particles in the size range of 200 and 400 nm. Non-AgI impurities reduced the INA of flare-generated particles ≤90 nm, which is lower than pure AgI particles ≤40 nm. The critical mass ice-active site density of the generated aerosols (*critical-n_m*) was derived, indicating the minimum mass of AgI particles required for efficient ice nucleation. The new parameterization to predict *critical-n_m* can serve as a reference to optimize the effectiveness of cloud-seeding materials for practical use.

Plain Language Summary Ice-forming aerosol is commonly added to clouds, expecting precipitation enhancement via promotion of ice production. In this work, silver iodide (AgI) containing aerosol was generated from commercial cloud-seeding products under different wind speed conditions. Its ice-forming ability was studied at mixed-phase cloud temperatures. The lower size limit for effective ice-forming ability of the cloud-seeding particles (90 nm) is higher than that of pure AgI particles (40 nm). The non-AgI components produced by cloud-seeding products are hypothesized to decrease the ice-forming ability of smaller particles, as the mass fraction of ice-nucleating AgI decreases. To estimate the minimum mass of AgI in a particle required for efficient ice nucleation under cloud-seeding relevant conditions, we derived the critical ice-activated mass fraction of the generated aerosols. These findings provide valuable insights into the optimization of cloud-seeding practices for enhanced precipitation.

1. Introduction

Ice crystals are important constituents of cold clouds (temperature <0°C) because their number concentration and size largely regulate cloud microphysics (Lamb, 2003) and impact cloud radiative properties and precipitation (Lohmann et al., 2016). Ice formation in the atmosphere can be initiated by the homogeneous freezing of supercooled cloud droplets (Koop et al., 2000) or via heterogeneous nucleation aided by ice-nucleating particles (INPs) (Cantrell & Heymsfield, 2005; Fletcher, 1970; Kanji et al., 2017; Murray et al., 2012). The presence of INPs lowers the energy barrier for ice embryos to form and facilitates a phase change under conditions where the homogeneous freezing rate is too low for freezing. If cloud droplets are artificially perturbed by the addition of INPs, the cloud microphysical processes are expected to change. As such INPs are of specific interest in weather modification to enhance precipitation (Rauber et al., 2019) or suppress hail (Dessens et al., 2016) by promoting ice production under appropriate meteorological and cloud water conditions. Ambiguous conclusions on the efficiency of previous cloud-seeding projects (French et al., 2018; Friedrich et al., 2020; Kerr, 1982; Manton & Warren, 2011; Pokharel et al., 2017; Rauber et al., 2019; Silverman, 2010) indicate that large uncertainties still exist in how INPs work under different meteorological conditions to influence cloud microphysics. For glaciogenic cloud seeding to work, the first step is to identify the ice nucleation ability (INA) of commercially available cloud-seeding aerosols.

Silver iodide (AgI) containing particles are widely used in cloud-seeding programs (French et al., 2018; Friedrich et al., 2020; Kerr, 1982; Manton & Warren, 2011; Pokharel & Geerts, 2016; Pokharel et al., 2017; Rauber et al., 2019; Silverman, 2010) due to its strong INA in the heterogeneous freezing regime (DeMott, 1995; Marcolli et al., 2016; Nagare et al., 2016; Vonnegut, 1947; Vonnegut, 1949). Laboratory experiments have been conducted to investigate the ice nucleation mechanism of pure AgI particles. The reason for its effect on ice nucleation is

imputed to its surface properties, including lattice matches with ice (Davis et al., 1975; Palanisamy et al., 1986), surface defects (Shevkunov, 2005, 2008), and surface charges (Edwards et al., 1962). AgI particles exhibit varying INAs when initiating ice formation through different pathways, as reviewed by Marcolli et al. (2016). The underlying mechanism behind the observed results is still debated.

The INAs of AgI-containing aerosols generated through different materials and methods were investigated and showed distinct results (Davis et al., 1975; DeMott et al., 1983; Edwards et al., 1962; Marcolli et al., 2016). The varied INAs are likely linked to the different physicochemical properties of the produced aerosols. AgI particles exhibit modified INAs after mixing with other chemical components (Davis et al., 1975; DeMott et al., 1983; Palanisamy et al., 1986). For example, an increase in INA has been observed for AgI particles after being mixed with AgCl or NaCl (DeMott et al., 1983; Palanisamy et al., 1986). These results imply the importance of the chemical composition of AgI-containing aerosols in altering their INAs. Particle size is another crucial characteristic affecting the INA of AgI particles. Larger AgI particles have a higher probability of hosting an ice active site on the surface and therefore nucleate ice more effectively compared to smaller particles at identical temperature and relative humidity conditions (DeMott, 1995; Edwards et al., 1962; Marcolli et al., 2016). The INA of AgI particles decreased significantly if sizes were <40 nm, attributed to the partial dissolution of AgI particles immersed in the cloud droplet (Marcolli et al., 2016).

In realistic cloud-seeding operations, the chemical composition and size distribution of cloud-seeding aerosol are determined by the composition of the seeding materials and the meteorological conditions where the seeding is conducted. Commercial cloud-seeding products contain non-AgI components that enable activation of particles into cloud droplets prior to freezing. These components have the potential to modify the chemical composition of cloud-seeding aerosol during its formation, although their exact impact on the INA of AgI particles remains unknown. The size distribution of the cloud-seeding aerosol is modulated by the encountered wind speeds, potentially playing a role in determining its INA. Nevertheless, the size distribution of cloud-seeding aerosols under varying wind speed conditions and the associated INAs have not been investigated so far. Other meteorological conditions including temperature and relative humidity in regions where cloud-seeding aerosols are deployed, will also influence their ice nucleation pathway and efficiency.

The above-mentioned results underscore the importance of the chemical nature and particle size in determining the INA of cloud-seeding aerosol in realistic cloud-seeding operations, which is less investigated and poorly understood. In this work, the immersion freezing of size-resolved AgI-containing aerosol was tested under mixed-phase cloud temperatures (243 K < T < 267 K) using a custom-designed ice nucleation chamber. The cloud-seeding aerosol was produced pyrotechnically from flares used in hail prevention programs in Switzerland under different wind speed conditions to test the effect of wind speed on the particle size distribution to mimic when flares are mounted on aircraft wings.

2. Methodology

The schematic of the experimental setup to generate the cloud-seeding aerosol, measure its size distribution and INA at 243 K < T < 270 K in the immersion freezing mode is shown in Figure S1 in Supporting Information S1.

2.1. Generation of Cloud-Seeding Aerosols

The AgI-containing aerosols were generated by igniting burn-in-place flares. The flare is a smaller and lower mass customized version of the burn-in-place ZEUS flares provided by Cloud Seeding Technologies for mounting on aircraft. The flares are composed of AgI (11.8%), iodine-containing compounds (15.3%) and other materials (such as ammonium perchlorate, catalysts, and fuel binder). The exact composition cannot be disclosed due to proprietary reasons. In each experiment, the investigated flare (7 mm in diameter) was fitted into the flare holder and ignited electronically in a customized fireproof burning chamber (BUC, Figure S2 in Supporting Information S1). The design of BUC is detailed in the supporting information (SI) (Figure S2, Text S1 in Supporting Information S1). Note that the unique design of the 3D-printed flare holder creates high wind speed conditions around flares (See Text S2 in Supporting Information S1 for working details), mimicking the wind conditions when flares are mounted on aircraft wings. Flare aerosol was produced at wind speeds of 25 m s^{-1} and 10 m s^{-1}, respectively. The generated aerosol was directed to a mixing tank after exhausting the first 20 s of burning (with a total burning time of approximately 90 s), after the burning stabilized. The mixing tank allows continued suspension of aerosol over a longer time for subsequent measurements of particle mass, size and ice

nucleation by different instruments. Two different mixing tanks were used to study particles of different sizes (see Text S3 in Supporting Information S1 for operational details).

2.2. Size Selection and Mass Measurement of Particles

The size distribution of the polydisperse aerosol particles was detected by a differential mobility particle spectrometer (DMPS) connected downstream of the tanks (see Text S4 in Supporting Information S1 for working details). The DMPS selected the monodisperse aerosol of one size (D_p). The total number concentration of the selected particles ($N_{total\ particles}$) entering the ice nucleation chamber was measured by a Condensation Particle Counter (TSI Inc., CPC 3772) positioned in front of the chamber, with a flow rate of 1 L min^{-1} (Figure S1 in Supporting Information S1). The monodisperse aerosol was sampled by the ice nucleation chamber (Figure S1 in Supporting Information S1). Occasionally, a centrifugal particle mass analyzer (CPMA, first generation, Cambustion Ltd.) with a flow rate of 1 L min^{-1} was connected to the monodisperse aerosol flow to measure the single-particle mass (see Text S5 in Supporting Information S1 for working details).

2.3. Ice Nucleation Measurements Under Mixed-Phase Cloud Conditions

The INA of the cloud-seeding aerosol was measured by the combination of an immersion mode cooling chamber (IMCA) (Lüönd et al., 2010) and the Zürich ice nucleation chamber (ZINC) (Stetzer et al., 2008), which has been used previously to investigate the immersion freezing of cloud droplets (Lüönd et al., 2010; Welti et al., 2019; Welti et al., 2012). Monodisperse aerosol was dried and sampled into IMCA with a relative humidity of ∼120% with respect to water (RH_w) (Figure S1 in Supporting Information S1). The high RH_w was caused by the temperature gradient (25 K) between the warm and cold walls of IMCA. The two vertically placed walls are lined with wetted filter papers, whose temperatures are controlled by two recirculating thermostats (Lauda, RP290). Particles activate and grow into cloud droplets (approximately 18∼20 μm in diameter) within a residence time of ∼10 s in IMCA and are then passed into the lower part of the IMCA where the temperature transitions ($T = 273$ K) to that of ZINC. ZINC is also a vertically oriented parallel plate chamber with ice-coated inner walls. The walls of ZINC are cooled to different temperatures to create a RH_w of 101%. The freezing fraction of droplets can be detected at 233 K < T < 270 K for a fixed humidity in this case. The residence time of particles in ZINC is ∼10 s. The total flow rate within the IMCA-ZINC system was kept at 10 L min^{-1} by an external pump (9 L min^{-1} of particle-free sheath air and 1 L min^{-1} of aerosol flow). The number concentration of particles was detected in situ by the Ice Optical Depolarization detector (IODE) (described in Nicolet et al. (2010)) mounted close to the exit of ZINC (Figure S1 in Supporting Information S1). IODE differentiates ice crystals and cloud droplets by depolarizing polarized light in the case of aspherical ice crystals. The frozen fraction (FF) of droplets is calculated based on the number concentration of ice crystals ($N_{ice\ crystals}$) and droplets ($N_{droplets}$) at the operational temperature conditions, as indicated by Equation 1:

$$FF = \frac{N_{ice\ crystals}}{N_{ice\ crystals} + N_{droplets}} \quad (1)$$

A higher FF represents higher INA of the tested particles.

The number concentrations of particles (0.5 ∼ 25 μm) were also detected by an optical particle counter (OPC, Lighthouse Remote 5,104) at the outlet of ZINC (Figure S1 in Supporting Information S1). An evaporation section with RH_i = 100% was attached downstream of IODE (Figure S1 in Supporting Information S1), forcing cloud droplets to evaporate before counting by the OPC. Only particles≥1.5 μm were defined as ice crystals. This threshold size was the maximum size that droplets can reach at a temperature slightly above homogeneous freezing (∼−34°C) after shrinking in the evaporation section, determined by measuring the phase transition of dilute ammonium nitrate droplets as a function of temperature. The activated fraction (AF) of aerosols was calculated by the ratio of the number concentration of ice crystals ($N_{ice\ crystals}$) determined by OPC and $N_{total\ particles}$ measured by CPC:

$$AF = \frac{N_{ice\ crystals}}{N_{total\ particles}} \quad (2)$$

The active site density per unit particle mass (n_m) can be estimated based on AF and the mass for a single particle measured by CPMA (M, Hiranuma et al. (2015)) or calculated by the particle diameter (D_p) and the particle density (ρ) by assuming a spherical particle shape ($M = \frac{\pi \rho {D_p}^3}{6}$) in the case of pure AgI particles.

$$n_m\,(T) = \frac{-\ln\,(1 - AF)}{M} \tag{3}$$

Similarly, the active site density per unit of particle surface (n_s) can be estimated based on AF and the surface area ($S = \pi {D_p}^2$) of spherical particles (Equation 4).

$$n_s\,(T) = \frac{-\ln\,(1 - AF)}{S} \tag{4}$$

The temperature performance of the IMCA-ZINC system was tested and validated before being used (see more details in Text S6 and Figure S5 in Supporting Information S1).

3. Results and Discussions

3.1. Size Distribution of Aerosols at Different Wind Speeds

Particle size distributions of the generated aerosols as a function of wind speed ($1 \sim 70$ m s^{-1}) was investigated as a separate experiment using a wind tunnel (Table S1 in Supporting Information S1). According to Table S1 in Supporting Information S1, particles of smaller size were produced under higher wind speed conditions. Additionally, it was shown that the size of the customized flare impacted the particle size distribution in a way that smaller particles were created with reduced flare diameters. The original commercial flare has a diameter of 24 mm and is usually operated at a wind speed of 70 m s^{-1} or even higher. The modal particle size generated under this condition is 52 nm (Table S1 in Supporting Information S1). To be as close to the particle size in real seeding conditions, the customized flare with a diameter of 7 mm (used in the present study) should be ignited at a wind speed of 30 m s^{-1} to obtain a similar mode size (52 nm, bold numbers in Table S1 in Supporting Information S1). Such a high wind speed condition could not be reached within the burning chamber under our laboratory conditions. The maximum wind speed of 25 m s^{-1} surrounding the flare was achieved in the end which profits from the unique design of the flare holder (Text S2 in Supporting Information S1).

The temporal evolution of particle size distribution generated at a wind speed of 25 m s^{-1} was monitored by the DMPS system (Figure 1). For comparison, the results obtained under a lower wind speed of 10 m s^{-1} are also depicted in Figure 1. In general, the sizes of the generated particles ranged from 60 to 700 nm and changed rapidly within the first 10 min after tank filling (Figures 1a and 1c). Particles <30 nm were exclusively generated at a wind speed of 25 m s^{-1} (Figures 1a and 11c), which is attributed to the high dispersion due to higher wind speeds. Smaller particles produced at higher wind speed are also observed in wind tunnel experiments (see Tabls S1 in Supporting Information S1). Thereafter, the particle size distribution shifted to larger sizes and stabilized for both applied wind speeds. The mode size reaches $400 \sim 500$ nm with a few particles <100 nm. A narrower particle size distribution was observed at a wind speed of 25 m s^{-1} after being stable ($300 \sim 700$ nm, Figure 1b and Figure S6 in Supporting Information S1) compared to that at a wind speed of 10 m s^{-1} ($100 \sim 700$ nm, Figure 1d and Figure S6 in Supporting Information S1). The total number concentration of the particles decreased over time (Figure S7 in Supporting Information S1). Initially, particle coagulation plays a role in a shift of the size distribution to larger sizes and reducing the total particle concentration. After $10 \sim 20$ min, continued dilution and wall losses further reduce the particle concentration. The coagulation also explained the larger particle size (>100 nm, Figure 1) obtained within the tank compared to those measured by wind tunnel (~50 nm, Table S1 in Supporting Information S1) under similar wind speed condition (~30 m s^{-1}), where the particles are homogeneously distributed in a continuous flow and have less chance to coagulate.

In general, the aerosol generated at a wind speed of 25 m s^{-1} was close to that produced under cloud-seeding wind conditions and thus was used for further ice nucleation measurements. Particles with distinct D_p of 90 nm, 200 and 400 nm were selected. The 90 nm particles were the smallest selectable and detectable particle size due to the rapid coagulation of smaller particles within the chamber. In addition, particles with a diameter of 200 and 400 nm were selected which represent the typical size range of the generated accumulation mode aerosol.

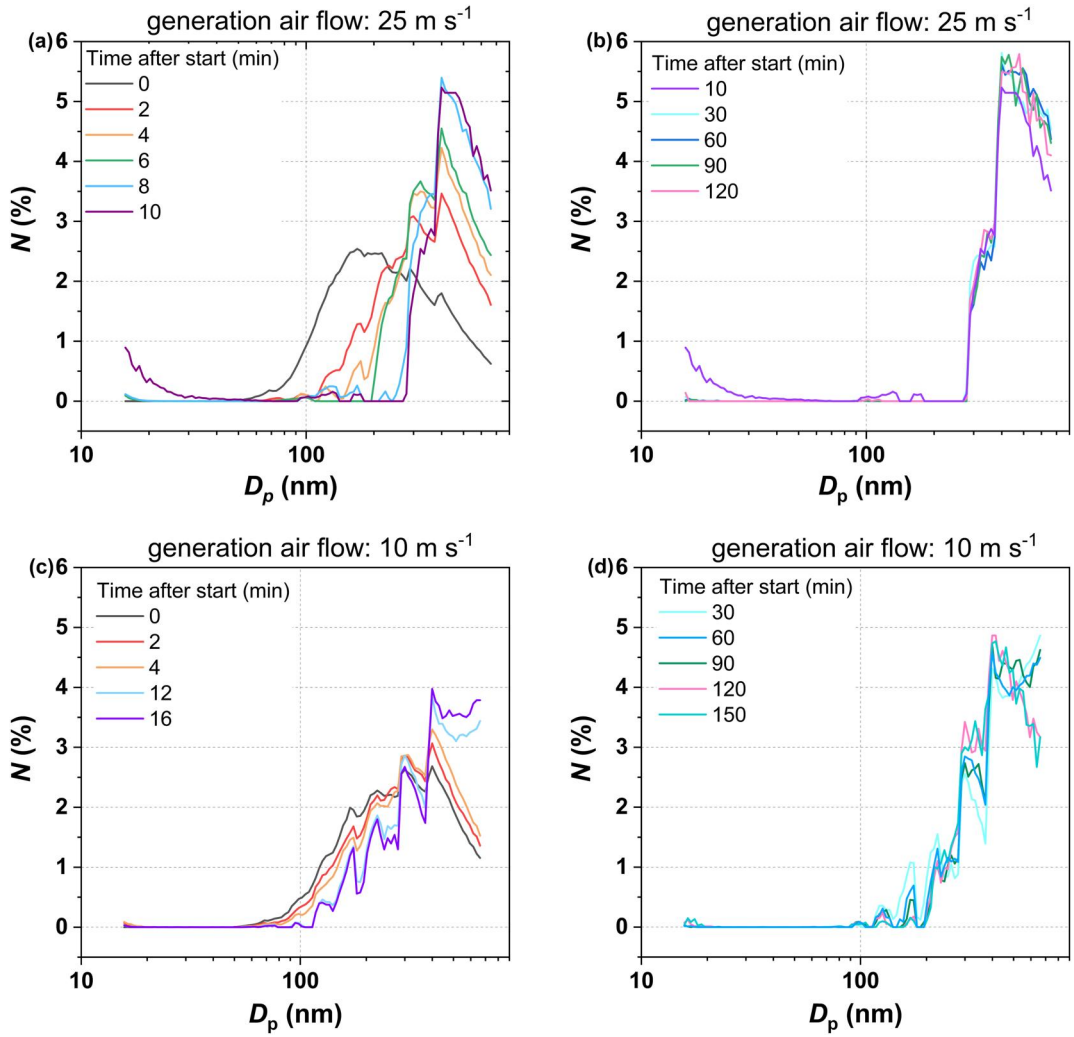

Figure 1. The temporal evolution of the number fraction (N (%)) of particles with different D_p measured at wind speeds of 25 m s^{-1} (panels a and b) and 10 m s^{-1} (panels c and d). Data for the first ~16 min (panels a and c) and up to 150 min after the start (panels b and d) are shown. "Time after start" represents the duration following the start of filling of the tank with aerosol.

3.2. INAs of Flare-Generated Aerosols

The FF of the particles as a function of temperature is shown in Figure 2. Error bars in Figure 2 indicate the uncertainties of FF, representing the deviation of FF at a given temperature for misclassifying a particle as an ice crystal versus a droplet in about 3,000 particles. Considering the uncertainties, FF of 200 and 400 nm particles are comparable at identical temperatures (244 K $\leq T \leq$ 267 K), while a lower FF was observed for 90 nm particles. This can also be observed by considering the temperature at which each particle size reaches a $FF \approx 1$. For the 90 nm, $FF \approx 1$ was reached at $T \approx 253$ K but for the 200 and 400 nm particles, $FF \approx 1$ was reached at 258 K (Figure 2a). This is expected because larger particles have a higher probability of containing an ice-active site with increasing particle surface and AgI mass. The lower INA of 90 nm flare-generated particles may be also attributed to some particle dissolution. As reported by Marcolli et al. (2016), AgI particles of smaller size would undergo dissolution after being immersed in cloud droplets, which leads to the erosion of the particle surface and reduction of its INA. They estimated a partial dissolution of 0.04% for 200 nm particles versus 38% for 20 nm particles, resulting in reduced INA for the latter. In our case, the dissolution for flare-generated particles is expected to be higher because of the overall lower AgI content of flare (~11.8% of the flare mass) resulting in a smaller mass of AgI in our cloud droplets compared to pure AgI particles immersed in a cloud droplet of the same size.

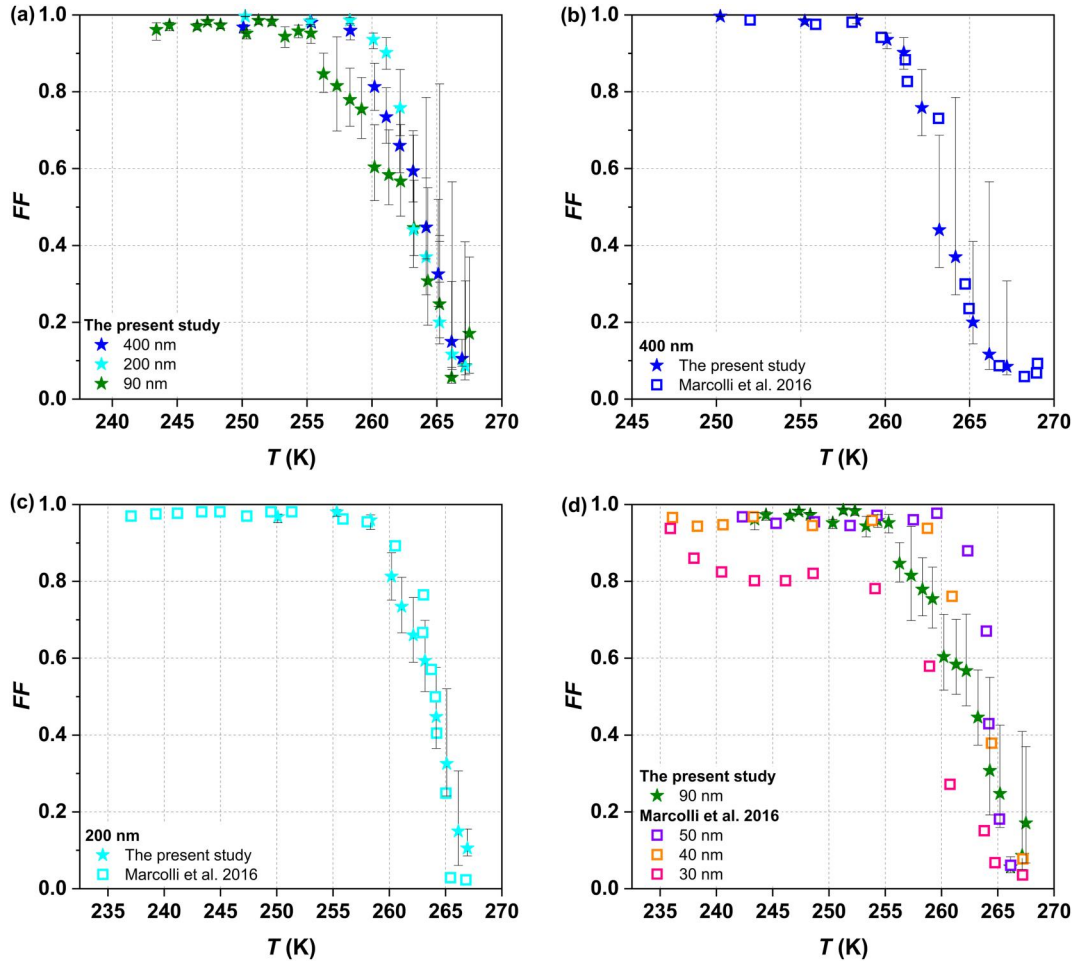

Figure 2. *FF* as a function of the temperature of flare-generated aerosols from this work (panel a) compared to those of similar sizes from Marcolli et al. (2016) (panels b, c and d). Stars represent flare-generated particles and diamond symbols represent the pure AgI particles generated from a AgI-water suspension (Marcolli et al., 2016). "Time after start" represents the duration following the start of filling of tank with aerosol.

The immersion freezing of flare-generated particles can be compared to those reported for AgI particles by Marcolli et al. (2016) (Figures 2b–2d). The AgI particles produced by Marcolli et al. (2016) can be approximated as pure AgI particles since the dissolved KNO_3 by-products was washed out before using the AgI particles for ice nucleation experiments (see more details in Nagare et al. (2015)) and will be used as a reference here. Similar to flare-generated particles, the *FF* of pure AgI particles shows a size-dependent INA below 50 nm (Figure 2d). AgI particles with sizes of 40 and 50 nm reach $FF \approx 1$ at 260 K, whereas 30 nm AgI particles reach $FF \approx 1$ at homogeneous freezing temperature ($T = 235$ K). Therefore, the critical size for AgI particles to nucleate ice efficiently is 40 nm, where the full INA potential ($FF \approx 1$) is reached before homogeneous freezing temperature. The pure AgI and flare-generated particles show excellent agreement in *FF* for the 200 and 400 nm size particles (Figures 2b and 2c). The INA of 90 nm flare-generated particles is lower than 40 nm but higher than 30 nm pure AgI particles (Figure 2d). The flare-generated particles contain other soluble components to promote droplet activation before freezing in real-world cloud-seeding operations. In particular, non-AgI components like ammonium perchlorate, and volatile compounds were produced upon burning. These impurities can either form non-AgI particles or condense onto the AgI particles such that a flare particle may not be composed entirely of AgI. At certain particle size, the ratio of AgI to non-AgI components would become critical to assessing the INA of flare-generated particles. Our results indicate that the critical size for flare-generated aerosol to nucleate ice efficiently is 90 nm, which includes sufficient AgI fraction comparable to that of 40 nm pure AgI particles (Figure 2d). Flare-generated particles <90 nm would have reduced INA due to an insufficient AgI content and the

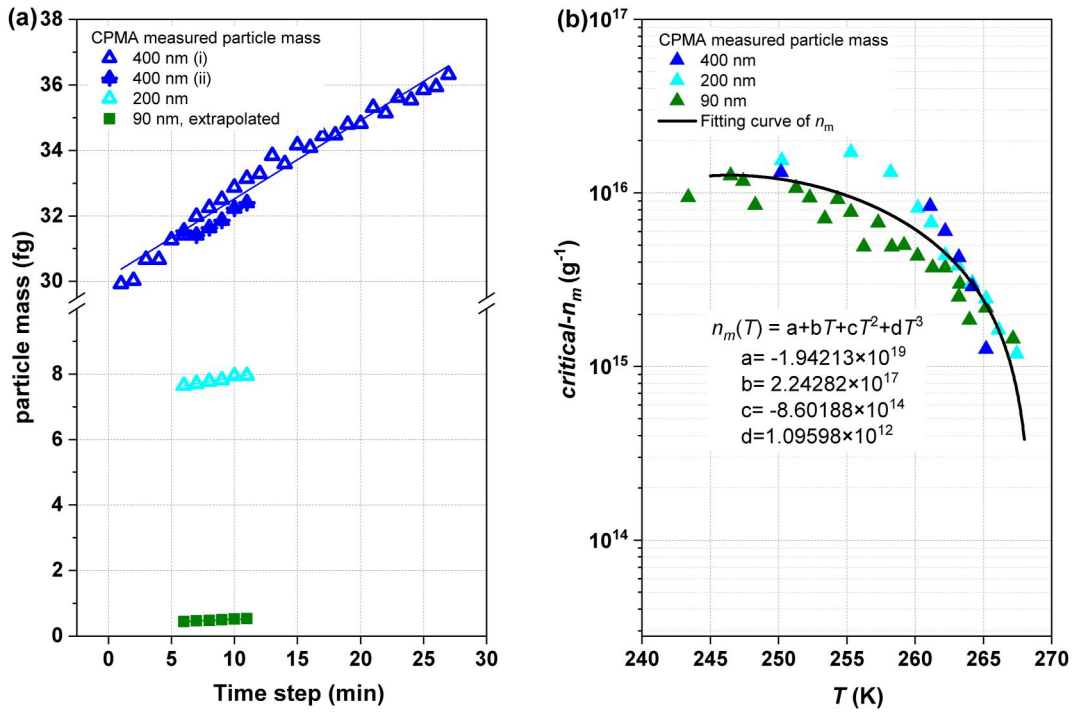

Figure 3. The change in particle mass over time measured by CPMA (a) and the derived critical ice active mass density of flare-generated particles (*critical-n_m*) (b). The solid line in (b) shows the parameterization to predict the *critical-n_m*, valid for 245 K < T < 267 (K).

increased partial dissolution, as evident by the significant decrease in INA observed for 30 nm AgI particles. In contrast, the effect of the non-AgI components on the INA of larger flare-generated particles (200 and 400 nm) is minor (Figure 2d), as their INA is similar to that of pure AgI ≥ 50 nm from Marcolli et al. (2016). In general, if the AgI content in flare-generated particles is higher than an equivalent 40 nm pure AgI particle (Figures 2b and 2c), their full ice nucleation potential is reached. We therefore recommend that cloud-seeding operation with aerosol from such burn-in-place flares should prioritize particles ≥90 nm. Moreover, effective cloud-seeding materials should contain a minimum AgI mass equivalent to 40 nm AgI particles to achieve the highest possible INA comparable to pure AgI particles.

DeMott (1995) investigated the INA of aerosols originating from burning AgI–acetone–ammonium iodide–water solutions in a propane flame. An appreciably lower freezing ability was observed for 30 and 70 nm particles compared to the 90 nm flare-generated particles in the present study and pure AgI particles (30 ~ 50 nm (Marcolli et al., 2016),) (Figure S8 in Supporting Information S1). The varied INAs of AgI-containing aerosols among studies, are evidence that the production method will impact the glaciogenic seeding ability of the particles that depend on the size and composition of the materials being used to generate the AgI aerosols. The characteristics of the additives and how they interact with the AgI particles will modify the INA of the generated aerosols. We cannot study the chemical composition of the flare-generated particles because of proprietary concerns. This may introduce uncertainty in estimating the critical AgI mass of flare-generated particles. To quantify the influence of non-AgI components on the INAs of cloud-seeding aerosols, further chemical characterization is required to identify their mass and mixing state with AgI. Nevertheless, we have found the flares used here have the closest INA to those of pure AgI particles, and thus could be effective for glaciogenic cloud seeding research and applications.

3.3. Critical Mass Activated Fraction (*Critical-n_m*) and Its Atmospheric Application

The change in mass for particles of fixed size over time is shown in Figure 3a. Since the decay in 90 nm particle number concentration occurred rapidly, the particle mass could not be detected. The 90 nm particle mass was calculated by the particle density derived from the measured average mass of 200 nm particles

assuming a spherical shape. The averaged particle mass with respect to the particle size is given in Table S2 in Supporting Information S1. The increase in particle mass over time (Figure 3a), confirms that by-products formed during the burning process were able to condense onto the AgI particle surfaces or smaller particles coagulated. Larger particles (200 and 400 nm) present a larger surface area but a smaller surface-to-volume ratio compared to smaller particles (90 nm). As a result, the ratio of the condensed by-products to AgI would be larger in smaller particles. As shown in Figure 3a, larger particles exhibit a mass ∼150 times higher than smaller particles after tank filling. This also explained why the condensation of by-products on larger particles did not lead to a reduced INA as observed with smaller particles, owing to the insufficient mass of by-products relative to AgI. The inhomogeneous chemical composition of flare-generated particles at different size and its impact on ice nucleation can also be seen in Figure S8 in Supporting Information S1 from the estimated mass ice active site density of particles (n_m) calculated by Equation 3 and the surface ice active site density of particles (n_s) calculated by Equation 4, where different n_m and n_s values were observed for particles of varying sizes. If particles had the same composition as a function of size, their INA should scale with surface area or mass and the normalized n_m or n_s values should fall onto a single curve, as observed by Welti et al. (2009) for illite clay particles (200 ∼ 800 nm).

From Figure S9 in Supporting Information S1 we can see that 90 nm particles give the highest INA of flare-generated particles is determined by a minimum effective AgI mass (equivalent to 40 nm AgI particle), above which larger particles (200 and 400 nm) or more AgI do not increase their INA. If n_m was derived based on the total mass of flare-generated particles, the ability of flare to produce INPs would be underestimated. Similarly, if n_m is scaled to masses above 40 nm AgI particle which do not additionally improve the INA, the n_m would also be underestimated. Based on these findings, we derive the critical ice active mass density (*critical-*n_m) from the measured flare-generated *FF* and the critical mass of 40 nm pure AgI particle (0.19 fg, calculated with a AgI particle density of 5.66 g cm^{-3}) required for efficient ice nucleation (Equation 3). The *critical-*n_m of all considered sizes can be fit by a curve that parameterizes the number of ice crystals produced per gram of seeding material. The new parameterization is displayed in Figure 3b, with a coefficient of determination (R^2) of 0.72. The substantial coefficient indicates the empirical data obtained aligns well with the values predicted by the proposed parameterization. The parameterization provides the expected ice crystal number produced per mass of seeding material as a function of seeding temperature, provided each seeding particle contains a minimum of 40 nm AgI. This parameterization has the potential to serve as a reference to optimize the production and efficiency of cloud-seeding materials in practical use. We note that in this work we only report on and support our data on the INA of the flare-generated aerosol, which is the first step for cloud seeding to be successful. The evolution of the seeded cloud, its dynamics and microphysics must be considered and researched further for various desired outcomes.

4. Conclusion

The INA of cloud-seeding aerosol was measured under mixed-phase cloud conditions (243 K < T < 267 K). The AgI-containing aerosol was produced by commercially available burn-in-place flares at a high wind speed (25 m s^{-1}), mimicking the aerosol generation process in real-world aircraft cloud-seeding operations. The flare-generated aerosols have comparable INA to pure AgI particles in the sizes of 200 and 400 nm. The non-AgI impurity produced from the same process lowers the INA of particles ≤90 nm, where the AgI mass is likely less than that of 40 nm pure AgI particles. If cloud-seeding particles in modes of 50–60 nm are produced due to high aircraft wind speeds, these particles will likely not contain enough AgI within them to achieve the full potential of glaciogenic seeding. Favoring flare-generated particles >90 nm is suggested to reach the full ice-seeding potential of the aerosol. For other cloud-seeding materials to reach a good INA, it is essential to include a minimum AgI mass equivalent to 40 nm AgI particles. The *critical-*n_m of the generated particles was estimated by normalizing the obtained *FF* with the mass of 40 nm AgI particles. *Critical-*n_m of all considered particle sizes agree well with each other and its temperature dependence can be described by a new parameterization valid for temperatures ranging from 245–267 K. This parameterization provides the minimum mass of AgI particles needed to produce the said ice crystal density. It holds significant potential in guiding the production and optimization of commercial seeding products.

Data Availability Statement

The data that support the conclusions of this study are available at Chen, (2023).

Acknowledgments
We acknowledge Mr. Frank Kasparek from Cloud Seeding Technologies for providing the commercial ZEUS flare. J.C. would also like to acknowledge the SNSF Swiss Postdoctoral Fellowships (SPF) grant TMPFP2_209830.

References

Cantrell, W., & Heymsfield, A. (2005). Production of ice in tropospheric clouds: A review. *Bulletin of the American Meteorological Society*, *86*(6), 795–808. https://doi.org/10.1175/bams-86-6-795

Chen, J. (2023). Data for ice nucleation measurement of cloud seeding aerosols [Dataset]. *Zenodo*. https://doi.org/10.5281/zenodo.8403462

Davis, B. L., Johnson, L. R., & Moeng, F. J. (1975). An explanation for the unusual nucleating ability of aerosols produced from the AgI-NH4I-acetone system. *Journal of Applied Meteorology and Climatology*, *14*(5), 891–896. https://doi.org/10.1175/1520-0450(1975)014<0891:aeftun>2.0.co;2

DeMott, P. J. (1995). Quantitative descriptions of ice formation mechanisms of silver iodide-type aerosols. *Atmospheric Research*, *38*(1), 63–99. https://doi.org/10.1016/0169-8095(94)00088-u

DeMott, P. J., Finnegan, W. G., & Grant, L. O. (1983). An application of chemical Kinetic theory and methodology to characterize the ice nucleating properties of aerosols used for weather modification. *Journal of Climate and Applied Meteorology*, *22*(7), 1190–1203. https://doi.org/10.1175/1520-0450(1983)022<1190:aaockt>2.0.co;2

Dessens, J., Sánchez, J. L., Berthet, C., Hermida, L., & Merino, A. (2016). Hail prevention by ground-based silver iodide generators: Results of historical and modern field projects. *Atmospheric Research*, *170*, 98–111. https://doi.org/10.1016/j.atmosres.2015.11.008

Edwards, G. R., Evans, L. F., & La Mer, V. K. (1962). Ice nucleation by monodisperse silver iodide particles. *Journal of Colloid Science*, *17*(8), 749–758. https://doi.org/10.1016/0095-8522(62)90049-1

Fletcher, N. H. (1970). *The chemical physics of ice*. Cambridge University Press.

French, J. R., Friedrich, K., Tessendorf, S. A., Rauber, R. M., Geerts, B., Rasmussen, R. M., et al. (2018). Precipitation formation from orographic cloud seeding. *Proceedings of the National Academy of Sciences*, *115*(6), 1168–1173. https://doi.org/10.1073/pnas.1716995115

Friedrich, K., Ikeda, K., Tessendorf, S. A., French, J. R., Rauber, R. M., Geerts, B., et al. (2020). Quantifying snowfall from orographic cloud seeding. *Proceedings of the National Academy of Sciences*, *117*(10), 5190–5195. https://doi.org/10.1073/pnas.1917204117

Hiranuma, N., Augustin-Bauditz, S., Bingemer, H., Budke, C., Curtius, J., Danielczok, A., et al. (2015). A comprehensive laboratory study on the immersion freezing behavior of illite NX particles: A comparison of 17 ice nucleation measurement techniques. *Atmospheric Chemistry and Physics*, *15*(5), 2489–2518. https://doi.org/10.5194/acp-15-2489-2015

Kanji, Z. A., Ladino, L. A., Wex, H., Boose, Y., Burkert-Kohn, M., Cziczo, D. J., & Krämer, M. (2017). Overview of ice nucleating particles. *Meteorological Monographs*, *58*(1.1), 1.1–1.33. https://doi.org/10.1175/amsmonographs-d-16-0006.1

Kerr, R. A. (1982). Cloud seeding: One success in 35 years. *Science*, *217*(4559), 519–521. https://doi.org/10.1126/science.217.4559.519

Koop, T., Luo, B., Tsias, A., & Peter, T. (2000). Water activity as the determinant for homogeneous ice nucleation in aqueous solutions. *Nature*, *406*(6796), 611–614. https://doi.org/10.1038/35020537

Lamb, D. (2003). Cloud microphysics. In J. R. Holton (Ed.), *Encyclopedia of atmospheric sciences* (pp. 459–467). Academic Press.

Lohmann, U., Lüönd, F., & Mahrt, F. (2016). *An introduction to clouds: From the microscale to climate*. Cambridge University Press.

Lüönd, F., Stetzer, O., Welti, A., & Lohmann, U. (2010). Experimental study on the ice nucleation ability of size-selected kaolinite particles in the immersion mode. *Journal of Geophysical Research*, *115*(D14). https://doi.org/10.1029/2009jd012959

Manton, M. J., & Warren, L. (2011). A confirmatory snowfall enhancement project in the snowy mountains of Australia. Part II: Primary and associated analyses. *Journal of Applied Meteorology and Climatology*, *50*(7), 1448–1458. https://doi.org/10.1175/2011jamc2660.1

Marcolli, C., Nagare, B., Welti, A., & Lohmann, U. (2016). Ice nucleation efficiency of AgI: Review and new insights. *Atmospheric Chemistry and Physics*, *16*(14), 8915–8937. https://doi.org/10.5194/acp-16-8915-2016

Murray, B. J., O'Sullivan, D., Atkinson, J. D., & Webb, M. E. (2012). Ice nucleation by particles immersed in supercooled cloud droplets. *Chemical Society Reviews*, *41*(19), 6519–6554. https://doi.org/10.1039/c2cs35200a

Nagare, B., Marcolli, C., Stetzer, O., & Lohmann, U. (2015). Comparison of measured and calculated collision efficiencies at low temperatures. *Atmospheric Chemistry and Physics*, *15*(23), 13759–13776. https://doi.org/10.5194/acp-15-13759-2015

Nagare, B., Marcolli, C., Welti, A., Stetzer, O., & Lohmann, U. (2016). Comparing contact and immersion freezing from continuous flow diffusion chambers. *Atmospheric Chemistry and Physics*, *16*(14), 8899–8914. https://doi.org/10.5194/acp-16-8899-2016

Nicolet, M., Stetzer, O., Lüönd, F., Möhler, O., & Lohmann, U. (2010). Single ice crystal measurements during nucleation experiments with the depolarization detector IODE. *Atmospheric Chemistry and Physics*, *10*(2), 313–325. https://doi.org/10.5194/acp-10-313-2010

Palanisamy, M., Thangaraj, K., Gobinathan, R., & Ramasamy, P. (1986). X-ray diffraction and ice nucleation studies of AgI□AgCl solid solutions. *Journal of Crystal Growth*, *79*(1, Part 2), 1005–1009. https://doi.org/10.1016/0022-0248(86)90587-7

Pokharel, B., & Geerts, B. (2016). A multi-sensor study of the impact of ground-based glaciogenic seeding on clouds and precipitation over mountains in Wyoming. Part I: Project description. *Atmospheric Research*, *182*, 269–281. https://doi.org/10.1016/j.atmosres.2016.08.008

Pokharel, B., Geerts, B., Jing, X., Friedrich, K., Ikeda, K., & Rasmussen, R. (2017). A multi-sensor study of the impact of ground-based glaciogenic seeding on clouds and precipitation over mountains in Wyoming. Part II: Seeding impact analysis. *Atmospheric Research*, *183*, 42–57. https://doi.org/10.1016/j.atmosres.2016.08.018

Rauber, R. M., Geerts, B., Xue, L., French, J., Friedrich, K., Rasmussen, R. M., et al. (2019). Wintertime orographic cloud seeding—A review. *Journal of Applied Meteorology and Climatology*, *58*(10), 2117–2140. https://doi.org/10.1175/jamc-d-18-0341.1

Shevkunov, S. V. (2005). Computer simulation of the initial stage of water vapor nucleation on a silver iodide crystal surface: 1. Microstructure. *Colloid Journal*, *67*(4), 497–508. https://doi.org/10.1007/s10595-005-0124-2

Shevkunov, S. V. (2008). Stimulation of vapor nucleation on perfect and imperfect hexagonal lattice surfaces. *Journal of Experimental and Theoretical Physics*, *107*(6), 965–983. https://doi.org/10.1134/s1063776108120078

Silverman, B. A. (2010). An evaluation of eleven operational cloud seeding programs in the watersheds of the Sierra Nevada Mountains. *Atmospheric Research*, *97*(4), 526–539. https://doi.org/10.1016/j.atmosres.2010.06.013

Stetzer, O., Baschek, B., Lüönd, F., & Lohmann, U. (2008). The Zurich Ice nucleation chamber (ZINC)-A new instrument to investigate atmospheric ice formation. *Aerosol Science and Technology*, *42*(1), 64–74. https://doi.org/10.1080/02786820701787944

Vonnegut, B. (1947). The nucleation of ice formation by silver iodide. *Journal of Applied Physics*, *18*(7), 593–595. https://doi.org/10.1063/1.1697813

Vonnegut, B. (1949). Nucleation of supercooled water clouds by silver iodide smokes. *Chemical Reviews*, *44*(2), 277–289. https://doi.org/10.1021/cr60138a003

Welti, A., Lohmann, U., & Kanji, Z. A. (2019). Ice nucleation properties of K-feldspar polymorphs and plagioclase feldspars. *Atmospheric Chemistry and Physics*, *19*(16), 10901–10918. https://doi.org/10.5194/acp-19-10901-2019

Welti, A., Lüönd, F., Kanji, Z. A., Stetzer, O., & Lohmann, U. (2012). Time dependence of immersion freezing: An experimental study on size selected kaolinite particles. *Atmospheric Chemistry and Physics*, *12*(20), 9893–9907. https://doi.org/10.5194/acp-12-9893-2012

Welti, A., Lüönd, F., Stetzer, O., & Lohmann, U. (2009). Influence of particle size on the ice nucleating ability of mineral dusts. *Atmospheric Chemistry and Physics*, *9*(18), 6705–6715. https://doi.org/10.5194/acp-9-6705-2009